



Article

Iontropic Gelation-Based Synthesis of Chitosan-Metal Hybrid Nanoparticles Showing Combined Antimicrobial and Tissue Regenerative Activities

Laura Lozano Chamizo ^{1,2,3}, Yurena Luengo Morato ¹, Karina Ovejero Paredes ^{1,2}, Rafael Contreras Caceres ⁴ , Marco Filice ^{1,2,*}  and Marzia Marciello ^{1,*}

¹ Nanobiotechnology for Life Sciences Laboratory, Department of Chemistry in Pharmaceutical Sciences, Faculty of Pharmacy, Universidad Complutense de Madrid (UCM), Plaza Ramón y Cajal s/n, 28040 Madrid, Spain; laurloza@ucm.es (L.L.C.); yluengo@ucm.es (Y.L.M.); kovejero@ucm.es (K.O.P.)

² Microscopy and Dynamic Imaging Unit, Fundación Centro Nacional de Investigaciones Cardiovasculares Carlos III (CNIC), Calle Melchor Fernández Almagro 3, 28029 Madrid, Spain

³ Atrys Health, 28001 Madrid, Spain

⁴ Department of Chemistry in Pharmaceutical Sciences, Faculty of Pharmacy, Universidad Complutense de Madrid (UCM), Plaza Ramón y Cajal s/n, 28040 Madrid, Spain; rafcontr@ucm.es

* Correspondence: mfilice@ucm.es (M.F.); marmarci@ucm.es (M.M.)



Citation: Lozano Chamizo, L.; Luengo Morato, Y.; Ovejero Paredes, K.; Contreras Caceres, R.; Filice, M.; Marciello, M. Iontropic Gelation-Based Synthesis of Chitosan-Metal Hybrid Nanoparticles Showing Combined Antimicrobial and Tissue Regenerative Activities. *Polymers* **2021**, *13*, 3910. <https://doi.org/10.3390/polym13223910>

Academic Editors: Barbara Viganò and Marzia Marciello

Received: 7 October 2021

Accepted: 8 November 2021

Published: 12 November 2021

Publisher's Note: MDPI stays neutral with regard to jurisdictional claims in published maps and institutional affiliations.



Copyright: © 2021 by the authors. Licensee MDPI, Basel, Switzerland. This article is an open access article distributed under the terms and conditions of the Creative Commons Attribution (CC BY) license (<https://creativecommons.org/licenses/by/4.0/>).

Abstract: The treatment of skin wounds poses significant clinical challenges, including the risk of bacterial infection. In particular due to its antimicrobial and tissue regeneration abilities chitosan (a polymeric biomaterial obtained by the deacetylation of chitin) has received extensive attention for its effectiveness in promoting skin wound repair. On the other hand, due to their intrinsic characteristics, metal nanoparticles (e.g., silver (Ag), gold (Au) or iron oxide (Fe₃O₄)) have demonstrated therapeutic properties potentially useful in the field of skin care. Therefore, the combination of these two promising materials (chitosan plus metal oxide NPs) could permit the achievement of a promising nanohybrid with enhanced properties that could be applied in advanced skin treatment. In this work, we have optimized the synthesis protocol of chitosan/metal hybrid nanoparticles by means of a straightforward synthetic method, ionotropic gelation, which presents a wide set of advantages. The synthesized hybrid NPs have undergone to a full physicochemical characterization. After that, the *in vitro* antibacterial and tissue regenerative activities of the achieved hybrids have been assessed in comparison to their individual constituent. As result, we have demonstrated the synergistic antibacterial plus the tissue regeneration enhancement of these nanohybrids as a consequence of the fusion between chitosan and metallic nanoparticles, especially in the case of chitosan/Fe₃O₄ hybrid nanoparticles.

Keywords: chitosan; gold; silver; iron oxide; nanoparticles; biomedical applications; nanotechnology; antimicrobial; skin regeneration; wound healing

1. Introduction

In the last decades, thanks to huge advances in nanotechnology, nanoparticles (NPs) have been widely studied for their application in biomedicine [1]. These NPs can be organic, inorganic or hybrid NPs, each of them offering different advantages and providing a wide range of applications in numerous fields [2–8]. Nowadays, the attention to hybrid NPs is increasing because they are more versatile and effective in overcoming obstacles compared to inorganic and/or organic ones alone [9–11]. The combination of inorganic and organic materials can lead to a synergistic effect or to a new hybrid nanosystem with unique properties [4,11,12]. These particles are being studied as carriers for drug delivery, gene therapy, imaging, theranosis, tissue regeneration, vaccines, among other uses [9].

In the context of tissue regeneration, skin cell regrowth is an interesting field considering that the integrity of healthy skin is crucial for maintaining human body's physiological

homeostasis [13,14]. Skin is the largest organ of human body, and thus highly vulnerable to a variety of damages and lesions, such as chronic wounds and deep burns of difficult healing [13]. These can affect millions of persons worldwide and can lead to serious clinical complications associated with long term hospitalization and expensive treatments without complete recovery of healthy skin conditions. Furthermore, many cutaneous injuries are followed by bacterial infection that can aggravate and slow down the skin regeneration process. Recent studies about tissue regeneration together with recent advances in the biomaterials and nanotechnology field, have been providing interesting and promising alternatives to the current treatments, offering the possibility of restoring the skin with its intrinsic functions [15–18]. Thus, in order to treat skin lesions, it is necessary to achieve wound closure and skin regeneration while avoiding bacterial infections [19]. To this aim, nanomedicine provides interesting and effective new tools to achieve this purpose [1,19]. Specifically, chitosan (CS)-based nanoparticles (NPs) have been revealed to be promising candidates for skin damage treatment [20].

Chitosan (CS) is a natural polysaccharide that shows interesting intrinsic properties such as biocompatibility, biodegradability, no antigenicity, mucoadhesive behaviour, anti-inflammatory and antibacterial abilities, making it an attractive material for biomedical applications [21–23]. Furthermore, recently, its ability to promote and accelerate tissue repair and regeneration processes was investigated [24].

On the other hand, inorganic NPs such as silver (Ag), gold (Au) or iron oxide (Fe_3O_4) NPs, have demonstrated promising properties related with tissue regeneration or wound healing, in addition to intrinsic therapeutic properties and the possibility of surface functionalization, useful to attach drugs or biomolecules for drug targeting [25].

Among different metal oxide nanoparticles, Fe_3O_4 NPs are well-known in the biomedical field because of their unique superparamagnetic properties and their different surface chemistry and functionalization. These were intensively applied for cell separation, tissue repair, targeted drug delivery (by using a magnet), bio-labelling material, hyperthermia and MRI contrast agents [2,26–31]. Furthermore, previous studies have reported that topically applied iron chelators and their novel therapeutic agents are able to improve the wound healing [32]. Recently, the antibacterial properties of these NPs have been studied in some depth [33,34], such as their application in regenerative medicine and tissue engineering [35], above all for neural and musculoskeletal tissues [36]. Thus, an interesting approach would be the incorporation of Fe_3O_4 NPs within CS polymeric NPs in order to combine their individual regenerative and antimicrobial properties in one unique element. In this sense, some examples of these synergistic effects have been reported although, in the vast majority of cases, only one bioactive property (antimicrobial or tissue regenerative) has been evaluated separately [37].

Ag NPs have demonstrated great potential in different biological applications, such as diagnosis, drug delivery, novel antimicrobial agents and regeneration materials [38–40]. In recent years, the antimicrobial behaviour of Ag NPs has led to increased demand for their applications in the biomedical field, including wound dressings, artificial implantation, and as antitumor drug carriers [41,42]. These NPs were also used as coatings for implantable medical devices, preventing infection and promoting wound healing, antibiotic delivery, microbial diagnostics, and antibacterial vaccines to control bacterial infections [43]. The main problem of these particles is associated to their cytotoxicity. Thus, a promising approach could be represented by the incorporation of Ag NPs into CS film matrices to minimize the severe toxicity of Ag NPs while maintaining or enhancing the antimicrobial effects [44–47].

Because of their unique surface, electronic and optical properties, Au NPs have been also widely used in biomedicine in areas such as biosensing, gene transfer and drug transport [11,48,49]. In the recent years, as a result of the nano-bio interaction with skin lipids, Au NPs have been shown to be capable of opening the stratum corneum and penetrating the skin barrier, so that their combination with CS would facilitate and improve their biological effects [50,51].

Therefore, the encapsulation of these inorganic NPs inside CS appears as an interesting and useful approach to investigate possible synergic effects between skin regeneration and wound healing while reducing eventual toxic side effects related to their nature.

To synthesize these hybrid NPs, different strategies have been described in literature [52]. However, the great majority of them require toxic crosslinkers (i.e., glutaraldehyde) and complex and not scalable strategies based on emulsification (with the use of harmful and organic solvents), reverse micelles (microemulsions) or phase inversion precipitation techniques among others [52–54]. In turn, little literature describing the application of the ionotropic gelation strategy for the synthesis of chitosan plus metal NPs hybrids has been published to date. Differently from the majority of reported strategies, this cheap, green and fully scalable method is based on a finely tuned and quick ionic crosslinking that involves the positive charges of chitosan and the negative charges of tripolyphosphate (TPP) in aqueous medium [55].

In this work, an accurate designed synthesis of CS-based hybrid NPs based on this green and simple synthetic strategy followed by an accurate physicochemical characterization will be described. As a result, a standard protocol based on an ionotropic gelation strategy for the preparation of hybrid CS/Fe₃O₄, CS/Ag and CS/Au NPs will be successfully optimized. After their physicochemical characterization, the biocompatibility, antimicrobial activity and tissue regeneration capability of the products will be studied and characterized for each hybrid.

2. Materials and Methods

2.1. Reagents

All the reagents used to synthesize polymeric and inorganic nanoparticles (NPs) were purchased from Merck (Darmstadt, Germany). These are: iron (III) chloride hexahydrate (FeCl₃·6H₂O), iron (II) chloride hydrate (FeCl₂·6H₂O), ammonium hydroxide (NH₄OH) and nitric acid (HNO₃) for iron oxide (Fe₃O₄) NPs, dodecylbenzene sulfonic acid (DBSA), aniline, silver nitrate (AgNO₃, ≥99%) for silver (Ag) NPs, HAuCl₄·3H₂O and trisodium citrate dehydrate for gold (Au) NPs, and chitosan (CS) (low molecular weight, 50–290 kDa and deacetylation degree of 75–85%) and sodium triphosphate pentabasic (TPP, ≥98%) for CS NPs synthesis. For cell culture and cell viability assays, Dulbecco's Modified Eagle's medium (DMEM) was obtained by Gibco (Waltham, MA, USA). Dimethylthiazolyl-diphenyl-tetrazolium bromide (MTT), dimethyl sulfoxide (DMSO) and FBS were bought by Merck. Finally, non-essential amino acids (NEAA) and sodium pyruvate were obtained from Hyclone (South Logan, UT, USA) while penicillin/streptomycin from Lonza (Basel, Switzerland).

2.2. Nanoparticles Synthesis

2.2.1. Iron Oxide Nanoparticles

Fe₃O₄ NPs were prepared following the Massart co-precipitation protocol with some modifications to control the particle size to 8 nm and to reduce the size distribution below a polydispersity degree of 0.2 (standard deviation/mean size) [56–58].

Briefly, magnetite (Fe₃O₄) NPs were prepared by fast co-precipitation (40 mL/s) of 425 mL of a mixture of FeCl₃·6H₂O (0.09 mol) and FeCl₂·6H₂O (0.054 mol) in 75 mL of alkaline medium (NH₄OH, 25%). After the synthesis, the particles were washed three times with distilled water in the presence of a permanent magnet. Then, an acid treatment was carried out, based on the oxidation of magnetite to maghemite (γ-Fe₂O₃), which is more stable in time and suitable for biomedical applications. 300 mL of HNO₃ (2 M) were added to the particles and stirred during 15 min. Then, the acid was removed by magnetic decantation, and 75 mL of Fe(NO₃)₃ (1 M) and 130 mL of water were added. The mixture was heated up to boiling temperature and stirred for 30 min. NPs were cooled to room temperature and after magnetic decantation (process in which a magnet is used to attract all magnetic components allowing their separation from a mixture), the supernatant was substituted by 300 mL of HNO₃ (2 M) and stirred for 15 min. Finally, the particles were

washed three times with acetone and redispersed in water, and a rotary evaporator was used to remove any acetone waste and concentrate the sample.

2.2.2. Silver Nanoparticles

Ag NPs were prepared following a previous described protocol [59]. Briefly, 3.48 g of DBSA were dissolved in 90 mL of distilled water, followed by the addition of 181 μL of aniline (186 mg) and vigorous stirring at 500 rpm until the solution took on a transparent, yellowish appearance. Then, 10 mL of a 0.2 M AgNO_3 aqueous solution were added and the resultant mixture was stirred for 15 min at 500 rpm. Next, this solution was heated to 90 °C in an oil bath and, when the temperature was reached, 4.5 mL of 3M NaOH aqueous solution were added. The mixture was kept at 90 °C for 1 h until a white AgCl precipitate was not observed when a 1 M NaCl solution was added to the reaction system, which implied almost the 100% yield reaction. The final colloidal dispersion was left to cool-down to room temperature and then was washed twice by centrifugation at 7500 rpm and 15 °C for 20 min. Then, the final Ag colloids were re-dispersed in distilled water.

2.2.3. Gold Nanoparticles

Au@citrate NPs were prepared following the Turkevich precipitation protocol in water [60]. Briefly, 95 mL of an aqueous solution containing 0.45 mM $\text{HAuCl}_4 \cdot 3\text{H}_2\text{O}$ was heated to boiling. Then, 5 mL of aqueous trisodium citrate solution (1g/100 L) was added under vigorous magnetic stirring. The initial yellowish solution changed immediately from colorless to black solution, and finally to a red wine color. Then, this colloidal dispersion was left to cool-down until room temperature and one part was washed by centrifugation at 6500 rpm and 15 °C for 5 min. Then, the final AuNPs colloids were re-dispersed in water (Au@citrate). The final Au concentration was calculated by the absorbance at 400 nm and confirmed by the inductively coupled plasma (ICP) technique.

2.2.4. Chitosan Nanoparticles

CS NPs were synthesized using the ionotropic gelation of CS with TPP method [61–64]. Briefly, CS was dissolved in an acid aqueous solution of 0.1% (*v/v*) acetic acid obtaining a dissolution of 1 mg/mL. Then, this solution was filtered by 0.45 μm using sterile filters and the pH was adjusted to 4.7–4.8. TPP was dissolved in distilled water in a concentration of 5 mg/mL and filtered by 0.22 μm using sterile filters. NPs were spontaneously formed by the incorporation of 1.2 mL of TPP solution in 3 mL of CS solution, under mild magnetic stirring at room temperature during 30 min. The prepared CS/TPP ratio resulted between 2.4/1 and 2.6/1 (*w/w*). To wash the synthesized NPs, the sample was centrifuged on a 4 μL of glycerol bed at 7000 rpm, 15 °C for 30 min, and resuspended in 100 μL of filtered distilled water after having discarded the supernatant.

2.2.5. Hybrid Nanoparticles

Hybrid CS-based NPs (CS/ Fe_3O_4 NPs, CS/Ag NPs and CS/Au NPs) were synthesized following a similar previously described protocol [55]. Briefly, 1.2 mL of TPP solution contained metal NPs in a concentration of 0.2 mg/mL were added to 1 mg/mL CS solution. The final CS/TPP ratio resulted in 2.6/1 (*w/w*) for the three hybrid samples. To wash the synthesized NPs, the sample was centrifuged on a 4 μL of glycerol bed at 7000 rpm, 15 °C for 30 min, and resuspended in 100 μL of filtered distilled water after having discarded the supernatant.

2.3. Nanoparticles Morphology, Size and Surface Zeta Potential Characterization

First, the morphology of all the synthesized NPs (metal, CS and hybrid NPs) was examined by transmission electron microscopy (TEM JEM 1400, JEOL, Akishima, Tokyo, Japan). Aqueous suspensions of the inorganic NPs were placed on 200 mesh copper grids coated with formvar/carbon without any staining. Colloidal suspensions of CS and hybrid samples were placed on the same grids after staining with 2% (*w/v*) of phosphotungstic

acid. The core size of each sample was achieved by using ImageJ program to measure the longer side of more than 200 nanoparticles. After that, all the values were processed by Origin obtaining the mean core size distribution (log-normal fit).

Measurements of NPs size and surface zeta potential were performed on freshly prepared and purified samples using a DLS Zetasizer Nano Zen 3600 (Malvern Instruments, Malvern, UK). For the particle size analysis, each sample was diluted to the appropriate concentration with filtered distilled water. And for the zeta potential analysis, samples were diluted in potassium nitrate (KNO₃, 0.01 M).

2.4. Fourier Transform Infrared (FTIR) Spectroscopy

FTIR measurements were carried out with lyophilized samples and were recorded using a Nicolet iS50 instrument (Thermo Fisher Scientific, Waltham, MA, USA) equipped with a KBr beam-splitter. The FTIR spectra were used to verify the formation of hybrid NPs.

2.5. Determination of Nanoparticles Synthesis Yield

The CS and hybrid NPs synthesis yield was determined by gravimetry. For this purpose, fixed volumes of NPs suspension were centrifuged at 7000 rpm, 15 °C for 30 min and, after that the supernatant was discarded, the pellets were lyophilized during 24 h using a LyoQuest (Telstar, Terrassa, Barcelona, Spain) lyophilizer and subsequently weighed. Three batches for each formulation were analysed.

2.6. Determination of Inorganic Nanoparticles Encapsulation

To determine the encapsulation grade of inorganic NPs in hybrid NPs, samples were centrifuged at 7000 rpm, 15 °C for 30 min and the supernatants and the pellets were separated for different analysis. First, pellets were lyophilized over 24 h using a LyoQuest (Telstar) lyophilizer and then analyzed by gravimetry. In addition, both pellets and corresponding supernatants were analyzed by the inductively coupled plasma (ICP, SPECTRO Arcos, SPECTRO, Kleve, Germany) technique to determine the concentration of metal NPs and, therefore, their encapsulation yield in the CS NPs.

2.7. Inorganic Nanoparticles Quantification

To determine Fe, Ag and Au amount in inorganic NPs, ICP analysis was used (as described in Section 2.6). Furthermore, Au and Fe concentrations were also measured by spectrophotometric methods. In more details, Au was determined measuring the absorbance at 400 nm. At this wavelength the main contribution to absorbance comes from absorption related to interband transitions in metallic gold which would thus be used to determine the amount of gold, regardless of particle size and shape. It has been reported that a value of 1.2 for the absorbance at 400 nm corresponds to an Au⁰ concentration of 0.5 mM [65].

For iron determination a Spectroquant Iron Test (Merck, Darmstadt, Germany) was used following the provider's instructions. All iron ions are reduced to iron (II) ions. In a thioglycolate-buffered medium these react with a triazine derivative to form a red-violet complex that is determined photometrically. Briefly, 40 µL of sample was digested with 40 µL of H₂O₂/HNO₃ (1:1.4) during 1 h at 60 °C. After digestion, the volume was adjusted to 5 mL with distilled water and 3 drops of kit reagent Fe-1 was added. This mixture was incubated for 3 min and then the absorbance was measured at 565 nm.

2.8. Cell Viability Assay

Mouse embryonic fibroblasts (MEF) were used to perform the cell viability assay, in order to study the toxicity of all the synthesized nanoparticles. This cell line was grown and maintained in DMEM supplemented with 10% FBS, 1% NEAA, 1% sodium pyruvate 100 mM and 1% penicillin/streptomycin. This culture was maintained at 37 °C and in an

atmosphere with 5% CO₂. Samples were redispersed in culture media, without phenol red, at different concentrations, and always sonicating repeatedly before cellular incubation.

Cells were seeded (4000 per well) in a 96-well culture plate and grown for 48 h at 37 °C. Then, cells were incubated for 24 h at 37 °C with different concentrations of each sample. After that, all the solutions were discarded and replaced by 100 µL of medium (without FBS and phenol red) and 10 µL of a 12 mM MTT solution in medium in each well. The reaction was incubated for 3 h, and then 85 µL of supernatants were removed, and 100 µL of DMSO were added to dissolve the formazan, leaving it 15 min in gentle agitation. Cell viability was estimated by measuring absorbance at 570 nm, knowing that the higher the absorbance, the higher the viability.

2.9. Antibacterial Activity Test

Antibacterial tests were carried out with bacteria in suspension (in planktonic state) with a single concentration of the different NPs samples. Briefly, 0.5 mL of bacterial suspension containing 2·10⁶ bacteria/mL of *Escherichia coli* in PBS 1X was placed in a 24-well culture plate together with 0.5 mL of the different NPs samples, in duplicate. This suspension was incubated for 4 h at 37 °C and continuous shaking. After this, 20 µL of a 1/1000 dilution from each well were seeded onto tryptic soy agar plates and incubated overnight at 37 °C. The next day, the colony formation on the different plates was checked.

2.10. Wound Healing Assay

MEF cells were seeded (35,000 per well) in a 24-well culture plate for 48 h, until a cell monolayer was created. The monolayer was scratched with a pipette tip and the medium was absorbed with vacuum. Then, the cells were incubated with the different samples (inorganic, CS and hybrid NPs) at different concentrations and the migration into the gap was imaged at 0, 24 and 48 h. Images were analysed in ImageJ (V 1.8.0, <https://imagej.nih.gov/ij/>) using the Wound Healing Tool.

3. Results and Discussion

3.1. Nanoparticles Preparation and Characterization

As first step, the metallic Ag, Au and Fe₃O₄ NPs were synthesized as described in the Material and Methods section, finally showing a core size of 33.02 nm (± 13.02 nm), 14.05 nm (± 1.61 nm) and 8.18 nm (± 1.57 nm), respectively, as measured by TEM microscopy (Figures 1c,e,g and S1; Table 1). When dispersed in aqueous medium, all the NPs tended to form small aggregates displaying hydrodynamic diameters of about 100 nm, 30 nm and 20 nm, respectively (analysed by the DLS technique, Table 1). In general, the metallic nanoparticles appear as spherical and monodisperse, except for Ag NPs that show a slightly higher polydispersity index (PDI = 0.29, Table 1).

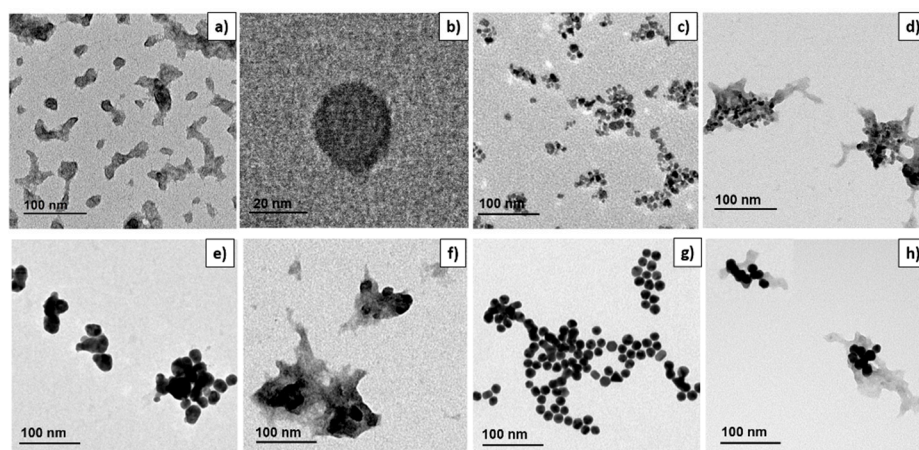


Figure 1. TEM micrographs of (a) CS NPs, (b) higher magnification of CS NPs, (c) Fe₃O₄ NPs, (d) hybrid CS/Fe₃O₄ NPs, (e) Ag NPs, (f) hybrid CS/Ag NPs, (g) Au NPS and (h) hybrid CS/Au NPs.

Table 1. Optimization study of ionotropic gelation-based synthesis of CS and CS-based hybrid NPs and their representative characterizations.

Sample	CS/TPP Ratio (w/w)	Core Size (nm)	Hydrodynamic Size (nm)	PDI *	ζ-Potential (mV) pH 7
CS NPs	2.4/1	33.7 ± 5.85	109.8	0.19	8.1
Fe ₃ O ₄ NPs	-	8.18 ± 1.57	19.98	0.18	3.6
CS/Fe ₃ O ₄ NPs	2.6/1	-	123.1	0.12	7.5
Ag NPs	-	33.02 ± 13.02	108.2	0.29	-11.8
CS/Ag NPs	2.5/1	-	121.8	0.22	7.7
Au NPs	-	14.05 ± 1.61	33.0	0.21	-17.4
CS/Au NPs	2.5/1	-	121.5	0.30	7.5

* PDI: Polydispersity Index.

After that, CS and hybrid NPs were prepared using the ionotropic gelation technique (Scheme 1a,b, respectively) [61]. As key parameter, various ratios between the constituents CS and TPP and/or inorganic NPs were studied to find the best relation for obtaining both the highest CS NPs yield and inorganic NPs encapsulation (Table 2). These conditions are related to polymer concentration. In fact, lower CS concentrations led to smaller size and higher yield due to mechanism of hybrid NPs formation [61]. Thanks to their amino groups that are positively charged at acid pH, CS chains are able to form an ionic network because of the crosslinking ability of negatively charged TPP [66] (Scheme 1).

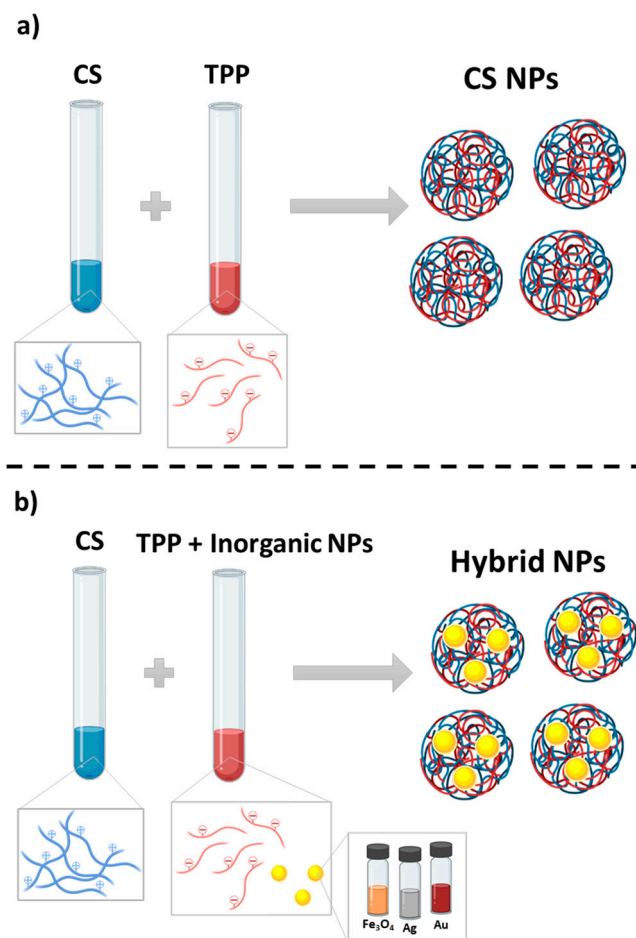
**Scheme 1.** General scheme for the synthesis of (a) CS NPs and (b) hybrid CS/Metal NPs. Created with BioRender.com.

Table 2. Yields of ionotropic gelation-based syntheses of CS and CS-based hybrid NPs and their chemical composition characterizations.

Sample	Inorganic NPs	Synthesis Yield (%)	Metal Encapsulation (%)	mg of Inorganic NPs in 1 mg/mL of Hybrid NPs	mg of CS in 1 mg of Hybrid NPs
CS NPs	-	65	-	-	1
CS/Fe ₃ O ₄ NPs	Fe ₃ O ₄	20	90.0	0.26	0.74
CS/Ag NPs	Ag	28	91.5	0.16	0.84
CS/Au NPs	Au	35	86.4	0.14	0.86

Hence, the highest yield (65%, Table 2) of CS NPs was obtained using a CS/TPP ratio of 2.4/1 (*w/w*). These NPs showed a spherical shape with a TEM core size of 34 nm (Figures 1a,b and S2). In aqueous medium, the CS NPs tend to form small aggregates with a hydrodynamic size around 100 nm (analysed by DLS technique) (Table 1). From the TEM micrographs in Figure 1a it is possible to observe that these CS NPs tend to form enlarged aggregates with an irregular necklace-shape. The aspect of these aggregated is in agreement with data reported in literature and could be correlated with similar sample-drying procedure, similar polymer molecular weight (MW) and similar deacetylation (DA) degree [67,68]. In fact, it was reported that bare CS NPs prepared by ionotropic gelation strategy and using CS with similar physical properties (MW and DA), showed the same shape (spherical) and the similar tendency to form similar necklace-shaped aggregates [68–74].

To promote their encapsulation within the polymeric matrix, the inorganic NPs were incorporated during the synthesis of CS NPs by means of their previous dispersion into the TPP solution. After testing different CS/TPP and TPP/inorganic NPs ratios (*w/w*), hybrid CS based NPs, with a hydrodynamic size of about 120 nm in all cases, were successfully prepared (Figure 1d,f,h; Table 1).

TEM micrographs show inorganic NPs inside CS NPs, confirming the successful encapsulation. These hybrid NPs are forming small aggregates with similar necklace shape to the CS ones. Nevertheless, the presence of some organic CS NPs (without encapsulated inorganic NPs), can be also appreciated demonstrating a no uniform distribution of inorganic NPs inside the CS. This behavior is mainly appreciable for Ag/CS and Au/CS NPs, probably due to the higher inorganic NPs core size than Fe₃O₄ NPs and to the inorganic NPs concentration used in the synthesis.

By applying the optimized conditions, the encapsulation of metal NPs was almost quantitative in all cases (Table 2). However, the overall yields of hybrid NPs were reduced with respect to bare CS NPs (from 65% to about 30%) (Table 2).

To confirm the successful formation of hybrid NPs as well as to quantify inorganic elements presence, surface ζ -potential, FT-IR and inductive coupled plasma (ICP) analyses were carried out.

At pH 7, the surface potential of hybrid NPs, was greatly increased from negative or near-to-zero values (−11.8 mV, −17.4 mV and 3.6 mV for Ag, Au and Fe₃O₄ NPs, respectively) to about +7.5 mV for all hybrid-based CS NP, demonstrating the successful inclusion of the metallic NPs within CS NPs (Table 2). In fact, the more positive ζ -potential is related to the presence of positive charged CS on hybrid NPs surface that finally masks the original negative charges. On the other hand, at the same pH value, the surface ζ -potential of CS NPs slightly decreased from 8.1 up to 7.5 mV as a consequence of the entrapment of the more negative metallic NPs within its structure (Table 2).

The isoelectric point of all the particles was also measured (Figure 2) and resulted almost the same (pH 8, approximatively, Figure 2c) for hybrid CS/metal NPs.

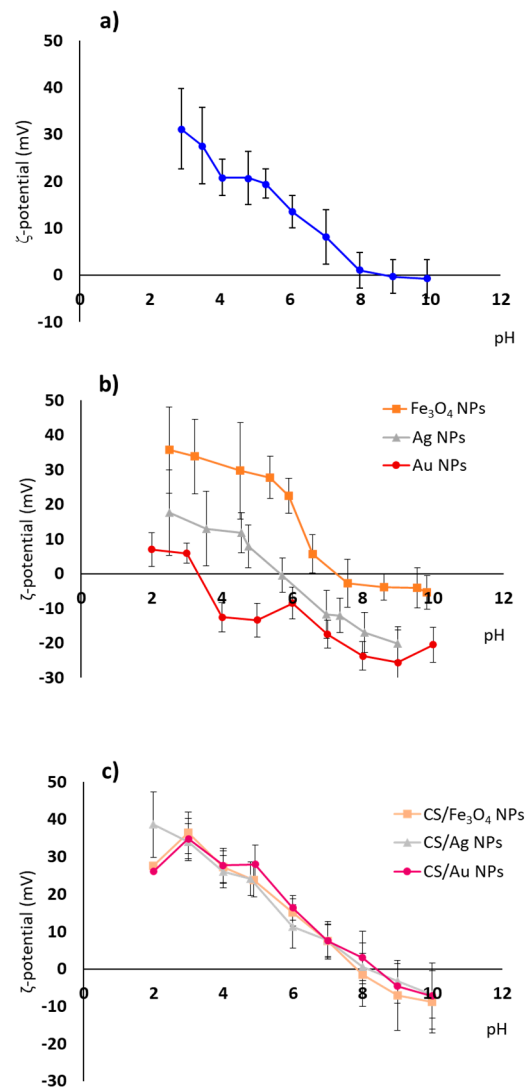


Figure 2. Surface ζ -Potential graphics of (a) CS NPs, (b) inorganic NPs and (c) hybrid CS-based NPs.

The FTIR spectra of CS and hybrid CS based NPs were recorded (Figure 3). The spectra of the polymer (CS) and each inorganic NP are reported in Supplementary Materials.

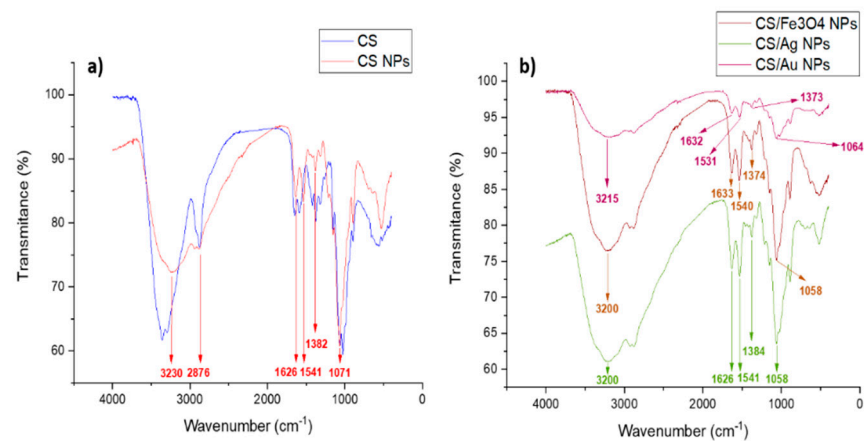


Figure 3. FT-IR spectra of (a) CS NPs compared to CS polymer and (b) hybrid CS based NPs.

More in details, Figure 3a shows the spectrum of CS NPs compared with the polymer alone. Pristine CS shows a band at 3363 cm^{-1} that was assigned to O–H and N–H group

stretching vibrations, while the band at 2876 cm^{-1} was due to the stretching vibrations of the aliphatic C–H bonds. The signals at 1642 cm^{-1} and 1583 cm^{-1} correspond to the stretching vibration of the amide bonds I, II and III. And the bands at 1377 cm^{-1} and 1024 cm^{-1} was assigned to C–N and C–O–C bonds, respectively (see Supplementary Materials). The peaks attributed to amide bonds shifted decreasing to 1626 cm^{-1} and 1541 cm^{-1} , which could be caused by the interaction between NH_3^+ groups of chitosan and phosphate groups of TPP [75]. The peak corresponding to O–H and N–H groups moved to 3230 cm^{-1} .

In Figure 3b, the FTIR spectra of hybrid NPs is reported. In CS/Ag NPs, the same peaks reported in CS NPs spectrum can be found with exception of the band at 3230 cm^{-1} of the O–H and N–H groups that decreased to 3200 cm^{-1} , suggesting the chelation of Ag with both amino and hydroxyl groups of chitosan. The same typical pattern can be observed in CS/ Fe_3O_4 and CS/Au NPs.

Thanks to the ICP-OES analysis, the amount of each metallic NP encapsulated within the CS polymeric matrix in each hybrid NPs was determined (Table 2). In more details, 0.26, 0.16 and 0.14 mg of Fe_3O_4 , AgNP and AuNPs, respectively, were included in 1 mg of each hybrid CS NPs. Altogether, all the reported characterizations confirmed the successful preparation of hybrid CS/metal NPs.

3.2. Cytotoxicity Tests

After a deep physicochemical characterization of all the synthesized NPs (inorganic, CS and hybrid NPs), with the aim of using these NPs in biomedical field, firstly their biocompatibility was tested in vitro. Fibroblasts cells (MEF) were chosen with the objective of testing all these nanomaterials as wound healing and skin regeneration tools. These cells have been selected for our studies as they show a pivotal role in the skin wound healing setting [76]. Thus, the demonstration of a potential proliferative activity with a concomitant moderate toxicity profile of our CS-based hybrid nanosystem on these cells could represent a very promising translational model.

In a first set of experiments, the potential cytotoxicity of all NPs on MEF cell line was assessed at different samples concentrations by using the MTT cell viability assay. As expected, CS NPs resulted non-toxic up to concentrations of 0.5 mg/mL being the final MEF availability at this concentration more than 75% (Figure S3). In turn, in comparison with CS NPs, inorganic NPs showed higher cytotoxicity both in their free and encapsulated forms (Figure 4). Fe_3O_4 NPs showed a behaviour similar to bare CS NPs, but up to a concentration of 0.1 mg/mL; at 0.25 mg/mL the cells' cytotoxicity increased. Biocompatibility of Au NPs was reduced to 60% at the concentration of 0.025 mg/mL while Ag NPs, at 0.0125 mg/mL, produced a 50% toxicity, showing the highest cytotoxicity values. Despite the toxicity of metal nanoparticles [77] and especially in the case of more toxic silver NPs, the incorporation of these inorganic NPs into CS network reduced their cytotoxicity, due to the presence of the most biocompatible CS layer on NPs surface. CS/ Fe_3O_4 NPs at a concentration of 0.08 mg/mL of Fe_3O_4 NPs showed a viability in cells of around 60%, having the same cell viability in the case of CS/Au NPs, at a concentration of 0.076 mg/mL of Ag NPs. These viabilities were almost the same in comparison with inorganic NPs alone. Nonetheless, the cell viability dropped up to 26% with a concentration of 0.068 mg/mL of free Ag NPs, while the cell viability was preserved at 41% at the same concentration of Ag NPs but encapsulated within the CS polymeric matrix, therefore, demonstrating the reduction of their cytotoxicity once in their CS-based hybrid form (Figure 4).

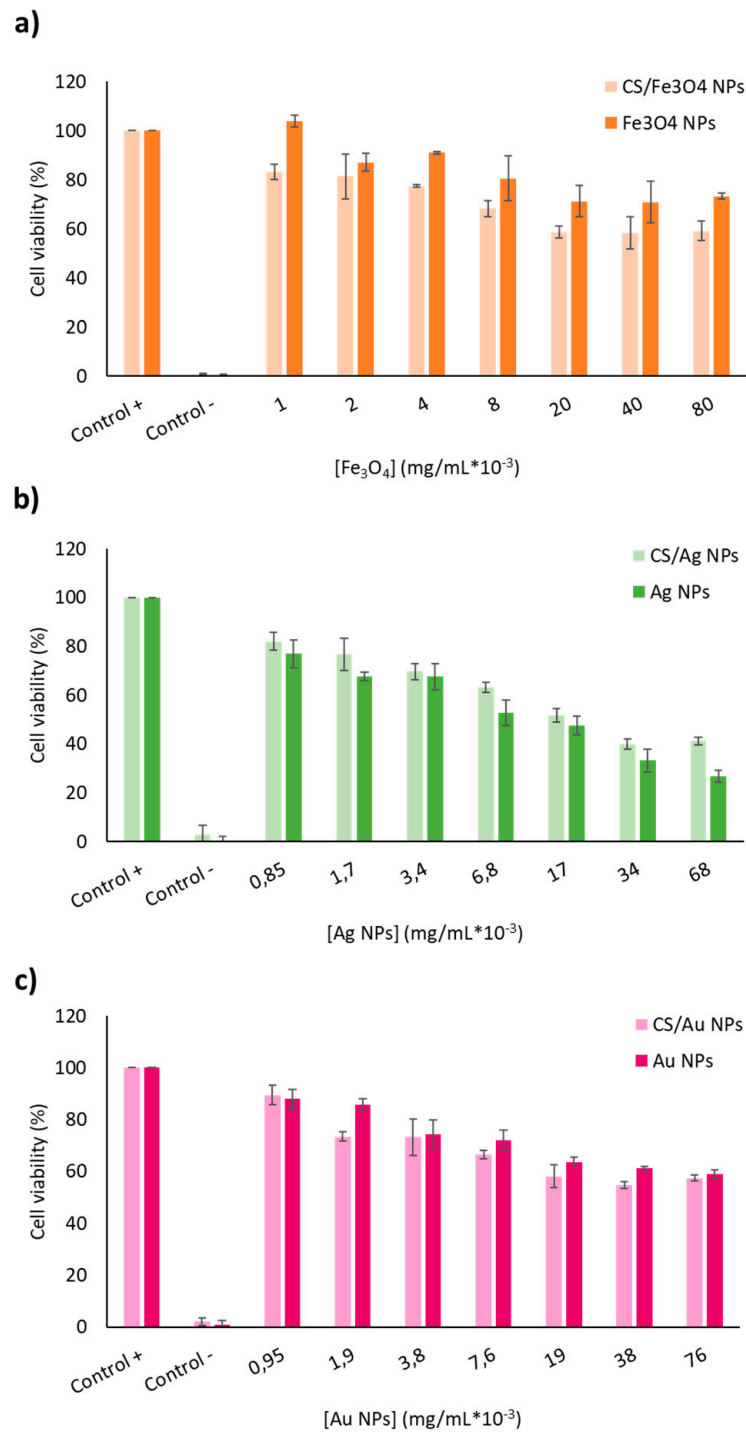


Figure 4. Cell viability assay of fibroblast as a function of different concentration of hybrid CS/metal nanoparticles versus free metal nanoparticles at the same concentration. (a) CS/Fe₃O₄ NPs versus free Fe₃O₄ NPs. (b) CS/Ag NPs versus free Ag NPs. (c) CS/Au NPs versus free Au NPs.

3.3. Antibacterial Activity Test

In order to assess the potential ability of these hybrid NPs to inhibit the bacterial growth, preliminary antibacterial tests were carried out on Gram negative *E. coli* as model. In fact, *Escherichia coli* strains frequently are isolated from skin and soft tissue infections [78]. To assess the antibacterial ability of CS NPs without impacting on its possible therapeutic ability, the highest no toxic concentration of CS NPs on MEF was tested (0.5 mg/mL). The same concentration of CS metal hybrid nanoparticles was applied in each case, and the

relative amount of free metal NPs contained in each hybrid (calculated by ICP, Table 2) was used as control (see Materials and Methods).

The results showed that bare CS NPs exhibited good antimicrobial properties as no *E. coli* colonies were formed on the plate upon incubation with the polymeric nanodrug (Figure 5). As expected, after incubation with free metallic nanoparticles, only AgNPs showed inhibitory activity while Fe₃O₄ NPs and AuNPs did not exert any antimicrobial activity as demonstrated by the *E. coli* colonies formation (Figure 5). In contrast, both inactive NPs (Fe₃O₄ and Au) turned in antimicrobial ones upon their encapsulation within the chitosan matrix. In fact, at the same metal concentration tested in their free form, both hybrids showed complete growth inhibition of *E. coli* colonies, therefore, confirming the raise of their antimicrobial ability (Figure 5) upon their hybridization with CS polymer. Altogether, these results clearly demonstrate the capability of CS/metal nanohybrids to inhibit bacterial growth thanks to presence of chitosan.

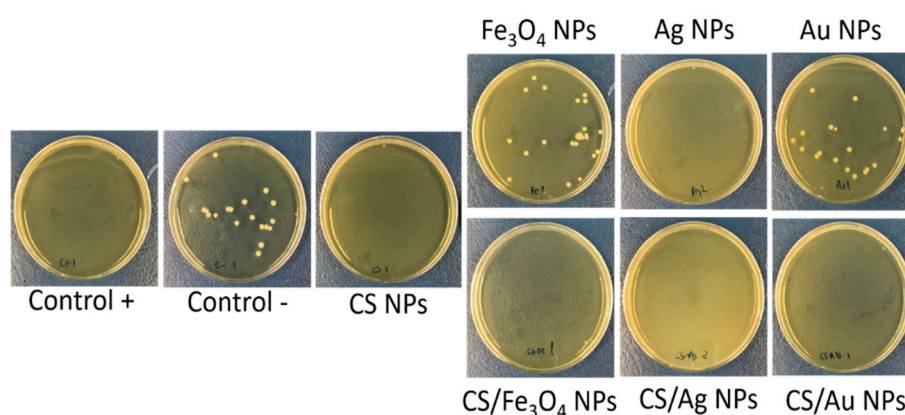


Figure 5. Antibacterial activity of CS based hybrid NPs compared to respective inorganic NPs measured by their ability to inhibit *E. coli* colonies formation.

3.4. Wound Healing Assay

Beside the antibacterial ability of our CS metal hybrid nanoparticles, we have also evaluated their potential capability to also promote, at the same time, skin wound healing [79]. Toward this end, we have carried out a scratch assay consisting in culturing MEF fibroblast in Petri dishes, generating a standard wound and assessing the ability of fibroblasts to heal that wound (in form of cell migration) in absence and in presence of each nanoparticle as well as of their individual constituent (Figures 6 and S4). The extent of cells' migration inside the scratch was measured by imaging analysis after 24 h and 48 h of incubation with the different NPs at different concentrations and comparing the residual wound area vs. the initial one. Upon analysis of all images recorded at all times and for each NPs at all concentrations studied, as general trend, it results clear that CS NPs and hybrid CS metal NPs promoted a faster wound healing process in comparison to the positive control (Figure S4). In more details, CS NPs at 33.75 µg/mL promoted 85% of scratch healing at 24 h and a quantitative healing at 48 h being 70% and 94% the healed areas at 24 h and 48 h, respectively, for positive control (Figure 6). Interestingly, at the same concentration, the CS/Fe₃O₄ NPs promoted the fastest cells migration with a quantitative wound healing after only 24 h (Figure 6). In the case of CS/Ag and CS/Au NPs, the appearance of this cell migration promotion activity was not appreciated (Figure S4). Therefore, besides the generation of antimicrobial activity, the hybridization between CS and Fe₃O₄ metal nanoparticles is able to also induce a tissue regenerative ability.

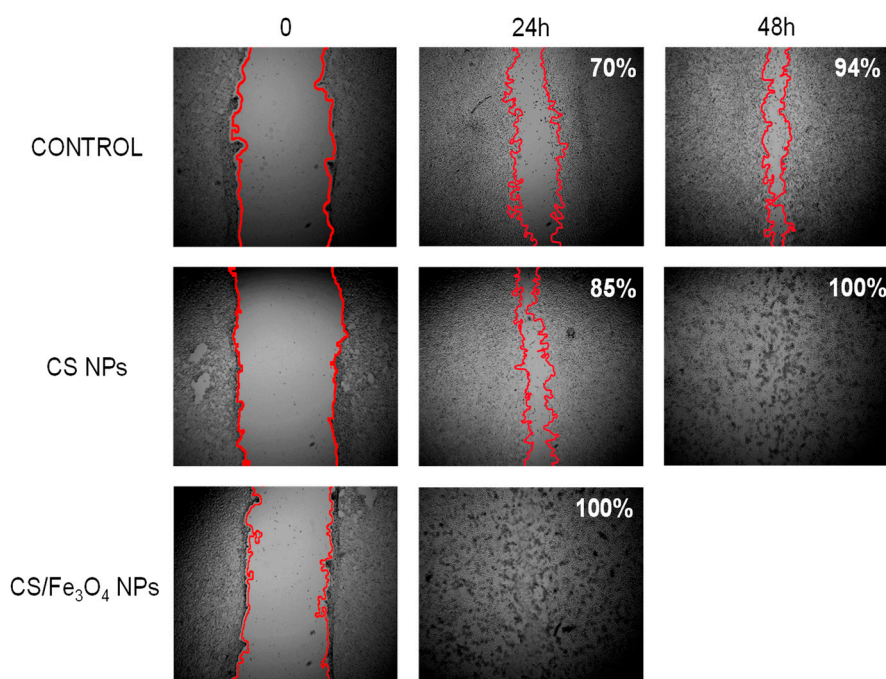


Figure 6. Hybrid NPs accelerated migration of fibroblast in scratch assay. Positive control at 0 h, 24 h and 48 h versus CS NPs (33.75 $\mu\text{g}/\text{mL}$) at 24 h and 48 h versus CS/ Fe_3O_4 NPs (33.75 $\mu\text{g}/\text{mL}$) at 24 h. The red lines indicate the fronts of migrating cells, and the percentage indicates the healed area.

4. Conclusions

In sum, in this work we have investigated the generation of a multifunctional hybrid nanoplatform composed by metallic nanoparticles embedded within a chitosan matrix. The goal of our strategy was to achieve a nanocomposite showing at the same time tissue regenerative and antimicrobial properties for its application in wounded skin management. The synthesis of the chitosan/metal hybrid nanoparticles has been carried out by means of the ionotropic gelation strategy. This green and practical synthetic protocol is characterized by its flexibility and scalability, thus, being a great added value toward its translational biomedical application. The achieved nanoparticles have been synthesised in good overall yield as a function of the ratio between the chitosan polymer, the TPP crosslinker and the amount of the metallic nanoparticles. The successful preparation of the nanohybrids has been confirmed in depth by different physico-chemical techniques (TEM, DLS, FTIR and ICP). After the physicochemical characterization, the biomedical activity of the bare CS NPs as well as of their hybrids with embedded metal nanoparticles was assessed. In general, all the CS-based nanoparticles showed good biocompatibility being the bare CS-NPs the most biocompatible ones. As a result of the entrapment of metal nanoparticles within the chitosan matrix, the CS metal hybrid nanoparticles acquired a good antibacterial activity. In fact, apart from AgNPs, the bare metal NPs did not show any initial antimicrobial activity. In addition to the antimicrobial activity, the combination between CS nanoparticles and Fe_3O_4 metal NPs metal hybrid also showed a good tissue regenerative activity as they promoted the fastest (24 h) and quantitative wound healing in fibroblast scratch model in comparison with the bare CS NPs and the CS Au and Ag hybrid nanoparticles. All together, these results indicate that, in terms of biocompatibility and combined antibacterial plus tissue regenerative activities, the CS/ Fe_3O_4 are the best hybrid nanoparticles synthesized by ionotropic gelation strategy. Therefore, this chitosan/iron nanocomposite can be considered as a very promising candidate for its biomedical applications in skin damage care.

Supplementary Materials: The following are available online at <https://www.mdpi.com/article/10.3390/polym13223910/s1>, Figure S1. TEM micrographs and size distribution (log-normal fit) of (a) iron oxide nanoparticles (IONPs), (b) silver nanoparticles (Ag NPs) and (c) gold nanoparticles (Au

NPs), Figure S2. TEM micrographs and size distribution (log-normal fit) of chitosan nanoparticles (CS NPs), Figure S3. Cytotoxicity assay of CS NPs in MEF cells, Figure S4. Wound healing assay of CS NPs and CS/metal hybrid NPs at 24 and 48 h.

Author Contributions: Conceptualisation, M.M. and M.F.; Data curation, L.L.C.; Investigation, L.L.C., Y.L.M., K.O.P. and R.C.C.; Supervision, M.M.; Writing—original draft, M.F. and M.M. All authors have read and agreed to the published version of the manuscript.

Funding: M.M., Y.L.M., and M.F. are grateful to the Comunidad Autonoma de Madrid and FEDER for the I + D collaborative Programme in Biomedicine NIETO-CM (Project reference B2017-BMD3731). M.F. and K.O.P. thank the Comunidad Autonoma de Madrid for research project No. 2017-T1/BIO-4992 (“Atracción de Talento” Action) cofunded by Universidad Complutense de Madrid. M.F. is grateful to Instituto de Salud Carlos III (ISCIII) for project No DTS20/00109 (AES-ISCIII). M.M., M.F. and L.L.C. would also like to thank Comunidad de Madrid for the predoctoral grant IND2020/BIO-17523. M.F. and K.O.P. acknowledge the support of Microscopy & Dynamic Imaging Unit of CNIC, Madrid, Spain. The Unit is part of the ReDiB-ICTS and has the support of FEDER, “Una manera de hacer Europa.” The CNIC is supported by MINECO and the Pro-CNIC Foundation and is a Severo Ochoa Centre of Excellence (SEV-2015-0505).

Institutional Review Board Statement: Not applicable.

Informed Consent Statement: Not applicable.

Data Availability Statement: Not applicable.

Acknowledgments: All the authors would like to thank Isabel Izquierdo-Barba, Blanca Gonzalez-Ortiz and Jesus Pablos-Lagartos (Department of Chemistry in Pharmaceutical Sciences, Faculty of Pharmacy, Universidad Complutense de Madrid (UCM)) for the practical assistance during the antimicrobial activity experiments.

Conflicts of Interest: The authors declare no conflict of interest.

References

1. Pelaz, B.; Alexiou, C.; Alvarez-Puebla, R.A.; Alves, F.; Andrews, A.M.; Ashraf, S.; Balogh, L.P.; Ballerini, L.; Bestetti, A.; Brendel, C.; et al. Diverse applications of nanomedicine. *ACS Nano* **2017**, *11*, 2313–2381. [[CrossRef](#)]
2. Marciello, M.; Pellico, J.; Fernandez-Barahona, I.; Herranz, F.; Ruiz-Cabello, J.; Filice, M. Recent advances in the preparation and application of multifunctional iron oxide and liposome-based nanosystems for multimodal diagnosis and therapy. *Interface Focus* **2016**, *6*, 20160055. [[CrossRef](#)]
3. Erami, R.S.; Ovejero, K.; Meghdadi, S.; Filice, M.; Amirnasr, M.; Rodriguez-Dieguez, A.; de La Orden, M.U.; Gomez-Ruiz, S. Applications of nanomaterials based on magnetite and mesoporous silica on the selective detection of zinc ion in live cell imaging. *Nanomaterials* **2018**, *8*, 434. [[CrossRef](#)] [[PubMed](#)]
4. Sanchez, A.; Ovejero Paredes, K.; Ruiz-Cabello, J.; Martinez-Ruiz, P.; Pingarron, J.M.; Villalonga, R.; Filice, M. Hybrid decorated core@ shell janus nanoparticles as a flexible platform for targeted multimodal molecular bioimaging of cancer. *ACS Appl. Mater. Interfaces* **2018**, *10*, 31032–31043. [[CrossRef](#)] [[PubMed](#)]
5. Vinambres, M.; Filice, M.; Marciello, M. Modulation of the catalytic properties of lipase b from candida antarctica by immobilization on tailor-made magnetic iron oxide nanoparticles: The key role of nanocarrier surface engineering. *Polymers* **2018**, *10*, 615. [[CrossRef](#)]
6. Filice, M.; Ruiz-Cabello, J. *Nucleic Acid Nanotheranostics: Biomedical Applications*; Elsevier: Amsterdam, The Netherlands, 2019.
7. Ovejero Paredes, K.; Diaz-Garcia, D.; Garcia-Almodovar, V.; Lozano Chamizo, L.; Marciello, M.; Diaz-Sanchez, M.; Prashar, S.; Gomez-Ruiz, S.; Filice, M. Multifunctional silica-based nanoparticles with controlled release of organotin metallodrug for targeted theranosis of breast cancer. *Cancers* **2020**, *12*, 187. [[CrossRef](#)] [[PubMed](#)]
8. Wang, L.; Marciello, M.; Estevez-Gay, M.; Soto Rodriguez, P.E.D.; Luengo Morato, Y.; Iglesias-Fernandez, J.; Huang, X.; Osuna, S.; Filice, M.; Sanchez, S. Enzyme conformation influences the performance of lipase-powered nanomotors. *Angew. Chem. Int. Ed. Engl.* **2020**, *59*, 21080–21087. [[CrossRef](#)]
9. Seaberg, J.; Montazerian, H.; Hossen, M.N.; Bhattacharya, R.; Khademhosseini, A.; Mukherjee, P. Hybrid nanosystems for biomedical applications. *ACS Nano* **2021**, *15*, 2099–2142. [[CrossRef](#)]
10. Taylor-Pashow, K.M.L.; Della Rocca, J.; Huxford, R.C.; Lin, W. Hybrid nanomaterials for biomedical applications. *Chem. Commun.* **2010**, *46*, 5832–5849. [[CrossRef](#)]
11. Luengo Morato, Y.; Marciello, M.; Lozano Chamizo, L.; Ovejero Paredes, K.; Filice, M. *Magnetic Nanoparticle-Based Hybrid Materials. Fundamentals and Applications. Cap 14: Hybrid Magnetic Nanoparticles for Multimodal Molecular Imaging of Cancer*; Elsevier: Amsterdam, The Netherlands, 2021.

12. Ferreira Soares, D.C.; Domingues, S.C.; Viana, D.B.; Tebaldi, M.L. Polymer-hybrid nanoparticles: Current advances in biomedical applications. *Biomed. Pharmacother.* **2020**, *131*, 110695. [[CrossRef](#)]
13. Chouhan, D.; Dey, N.; Bhardwaj, N.; Mandal, B.B. Emerging and innovative approaches for wound healing and skin regeneration: Current status and advances. *Biomaterials* **2019**, *216*, 119267. [[CrossRef](#)] [[PubMed](#)]
14. Kimura, S.; Tsuchiya, A.; Ogawa, M.; Ono, M.; Suda, N.; Sekimoto, K.; Takeo, M.; Tsuji, T. Tissue-scale tensional homeostasis in skin regulates structure and physiological function. *Commun. Biol.* **2020**, *3*, 637. [[CrossRef](#)] [[PubMed](#)]
15. Bellu, E.; Medici, S.; Coradduzza, D.; Cruciani, S.; Amler, E.; Maioli, M. Nanomaterials in skin regeneration and rejuvenation. *Int. J. Mol. Sci.* **2021**, *22*, 7095. [[CrossRef](#)]
16. Mohammadzadeh, L.; Mahkam, M.; Barzegari, A.; Karimi, A.; Kafil, H.S.; Salehi, R.; Rahbarghazi, R. Preparation, characterization, and antibacterial properties of hybrid nanofibrous scaffolds for cutaneous tissue engineering. *Hum. Cell* **2021**, *34*, 1682–1696. [[CrossRef](#)] [[PubMed](#)]
17. Badawy, M.E.I.; Lotfy, T.M.R.; Shawir, S.M.S. Preparation and antibacterial activity of chitosan-silver nanoparticles for application in preservation of minced meat. *Bull. Natl. Res. Cent.* **2019**, *43*, 83. [[CrossRef](#)]
18. Moreira, H.R.; Marques, A.P. Vascularization in skin wound healing: Where do we stand and where do we go? *Curr. Opin. Biotechnol.* **2022**, *73*, 253–262. [[CrossRef](#)]
19. Wang, W.; Lu, K.-j.; Yu, C.-h.; Huang, Q.-l.; Du, Y.-Z. Nano-drug delivery systems in wound treatment and skin regeneration. *J. Nanobiotechnol.* **2019**, *17*, 82. [[CrossRef](#)]
20. Sultankulov, B.; Berillo, D.; Sultankulova, K.; Tokay, T.; Saparov, A. Progress in the development of chitosan-based biomaterials for tissue engineering and regenerative medicine. *Biomolecules* **2019**, *9*, 470. [[CrossRef](#)]
21. Zhao, D.; Yu, S.; Sun, B.; Gao, S.; Guo, S.; Zhao, K. Biomedical applications of chitosan and its derivative nanoparticles. *Polymers* **2018**, *10*, 462. [[CrossRef](#)]
22. Rossi, S.; Marciello, M.; Sandri, G.; Bonferoni, M.C.; Ferrari, F.; Caramella, C. Chitosan ascorbate: A chitosan salt with improved penetration enhancement properties. *Pharm. Dev. Technol.* **2008**, *13*, 513–521. [[CrossRef](#)]
23. Rossi, S.; Marciello, M.; Sandri, G.; Ferrari, F.; Bonferoni, M.C.; Papetti, A.; Caramella, C.; Dacarro, C.; Grisoli, P. Wound dressings based on chitosans and hyaluronic acid for the release of chlorhexidine diacetate in skin ulcer therapy. *Pharm. Dev. Technol.* **2007**, *12*, 415–422. [[CrossRef](#)] [[PubMed](#)]
24. Feng, P.; Luo, Y.; Ke, C.; Qiu, H.; Wang, W.; Zhu, Y.; Hou, R.; Xu, L.; Wu, S. Chitosan-based functional materials for skin wound repair: Mechanisms and applications. *Front. Bioeng. Biotechnol.* **2021**, *9*, 650598. [[CrossRef](#)] [[PubMed](#)]
25. Khalid, K.; Tan, X.; Mohd Zaid, H.F.; Tao, Y.; Lye Chew, C.; Chu, D.T.; Lam, M.K.; Ho, Y.C.; Lim, J.W.; Chin Wei, L. Advanced in developmental organic and inorganic nanomaterial: A review. *Bioengineered* **2020**, *11*, 328–355. [[CrossRef](#)]
26. Li, X.; Wang, Y.; Shi, L.; Li, B.; Li, J.; Wei, Z.; Lv, H.; Wu, L.; Zhang, H.; Yang, B.; et al. Magnetic targeting enhances the cutaneous wound healing effects of human mesenchymal stem cell-derived iron oxide exosomes. *J. Nanobiotechnol.* **2020**, *18*, 113. [[CrossRef](#)]
27. Branca, M.; Marciello, M.; Ciuculescu-Pradines, D.; Respaud, M.; Morales, M.d.P.; Serra, R.; Casanove, M.-J.; Amiens, C. Towards MRI T2 contrast agents of increased efficiency. *J. Magn. Magn. Mater.* **2015**, *377*, 348–353. [[CrossRef](#)]
28. Kossatz, S.; Ludwig, R.; Dähring, H.; Ettelt, V.; Rimkus, G.; Marciello, M.; Salas, G.; Patel, V.; Teran, F.J.; Hilger, I. High therapeutic efficiency of magnetic hyperthermia in xenograft models achieved with moderate temperature dosages in the tumor area. *Pharm. Res.* **2014**, *31*, 3274–3288. [[CrossRef](#)] [[PubMed](#)]
29. Lazaro-Carrillo, A.; Filice, M.; Guillén, M.J.; Amaro, R.; Viñambres, M.; Tabero, A.; Paredes, K.O.; Villanueva, A.; Calvo, P.; del Puerto Morales, M.; et al. Tailor-made PEG coated iron oxide nanoparticles as contrast agents for long lasting magnetic resonance molecular imaging of solid cancers. *Mater. Sci. Eng. C* **2020**, *107*, 110262. [[CrossRef](#)] [[PubMed](#)]
30. Palma, S.I.; Carvalho, A.; Silva, J.; Martins, P.; Marciello, M.; Fernandes, A.R.; del Puerto Morales, M.; Roque, A.C. Covalent coupling of gum arabic onto superparamagnetic iron oxide nanoparticles for MRI cell labeling: Physicochemical and in vitro characterization. *Contrast Media Mol. Imaging* **2015**, *10*, 320–328. [[CrossRef](#)]
31. Luengo Morato, Y.; Ovejero Paredes, K.; Lozano Chamizo, L.; Marciello, M.; Filice, M. Recent advances in multimodal molecular imaging of cancer mediated by hybrid magnetic nanoparticles. *Polymers* **2021**, *13*, 2989. [[CrossRef](#)]
32. Yadav, E.; Yadav, P.; Verma, A. In silico study of trianthema portulacastrum embedded iron oxide nanoparticles on glycogen synthase kinase-3beta: A possible contributor to its enhanced in vivo wound healing potential. *Front. Pharmacol.* **2021**, *12*, 664075. [[CrossRef](#)]
33. Ismail, R.A.; Sulaiman, G.M.; Abdulrahman, S.A.; Marzoog, T.R. Antibacterial activity of magnetic iron oxide nanoparticles synthesized by laser ablation in liquid. *Mater. Sci. Eng. C Mater. Biol. Appl.* **2015**, *53*, 286–297. [[CrossRef](#)]
34. Saqib, S.; Munis, M.F.H.; Zaman, W.; Ullah, F.; Shah, S.N.; Ayaz, A.; Farooq, M.; Bahadur, S. Synthesis, characterization and use of iron oxide nano particles for antibacterial activity. *Microsc. Res. Tech.* **2019**, *82*, 415–420. [[CrossRef](#)] [[PubMed](#)]
35. Friedrich, R.P.; Cicha, I.; Alexiou, C. Iron oxide nanoparticles in regenerative medicine and tissue engineering. *Nanomaterials* **2021**, *11*, 2337. [[CrossRef](#)]
36. Nanda, T.; Alobaid, M.; Rege, K. Iron oxide nanoparticles for tissue repair and regeneration. *Nano LIFE* **2021**, *11*, 2030001. [[CrossRef](#)]
37. Arakha, M.; Pal, S.; Samantarrai, D.; Panigrahi, T.K.; Mallick, B.C.; Pramanik, K.; Mallick, B.; Jha, S. Antimicrobial activity of iron oxide nanoparticle upon modulation of nanoparticle-bacteria interface. *Sci. Rep.* **2015**, *5*, 14813. [[CrossRef](#)] [[PubMed](#)]

38. Burdusel, A.C.; Gherasim, O.; Grumezescu, A.M.; Mogoanta, L.; Ficai, A.; Andronesu, E. Biomedical applications of silver nanoparticles: An up-to-date overview. *Nanomaterials* **2018**, *8*, 681. [[CrossRef](#)] [[PubMed](#)]
39. Gunasekaran, T.; Nigusse, T.; Dhanaraju, M.D. Silver nanoparticles as real topical bullets for wound healing. *J. Am. Coll. Clin. Wound Spec.* **2012**, *3*, 82–96. [[CrossRef](#)] [[PubMed](#)]
40. Luengo, Y.; Sot, B.; Salas, G. Combining Ag and γ -Fe(2)O(3) properties to produce effective antibacterial nanocomposites. *Colloids Surf. B Biointerfaces* **2020**, *194*, 111178. [[CrossRef](#)]
41. Nešporová, K.; Pavlík, V.; Šafránková, B.; Vágnerová, H.; Odráška, P.; Žídek, O.; Císařová, N.; Skoroplyas, S.; Kubala, L.; Velebný, V. Effects of wound dressings containing silver on skin and immune cells. *Sci. Rep.* **2020**, *10*, 15216. [[CrossRef](#)] [[PubMed](#)]
42. Rozalen, M.; Sánchez-Polo, M.; Fernández-Perales, M.; Widmann, T.J.; Rivera-Utrilla, J. Synthesis of controlled-size silver nanoparticles for the administration of methotrexate drug and its activity in colon and lung cancer cells. *RSC Adv.* **2020**, *10*, 10646–10660. [[CrossRef](#)]
43. Wang, L.; Hu, C.; Shao, L. The antimicrobial activity of nanoparticles: Present situation and prospects for the future. *Int. J. Nanomed.* **2017**, *12*, 1227–1249. [[CrossRef](#)]
44. Abaza, S.F.; Elbially, N.S.; Mohamed, N. Incorporating silver nanoshell-coated mesoporous silica nanoparticles improves physicochemical and antimicrobial properties of chitosan films. *Int. J. Biol. Macromol.* **2021**, *189*, 792–801. [[CrossRef](#)]
45. Chen, Z.; Yuan, J.; Yu, Q.; Luo, Z.; Xie, C.; Zhang, K.; Tang, L.; Wang, H. High strength antibacterial membranes consisted of nanofibrous chitosan immobilized silver nanoparticles. *J. Appl. Polym. Sci.* **2021**, *138*. [[CrossRef](#)]
46. Chen, X.; Zhang, H.; Yang, X.; Zhang, W.; Jiang, M.; Wen, T.; Wang, J.; Guo, R.; Liu, H. Preparation and application of quaternized chitosan- and agnps-base synergistic antibacterial hydrogel for burn wound healing. *Molecules* **2021**, *26*, 4037. [[CrossRef](#)]
47. You, C.; Li, Q.; Wang, X.; Wu, P.; Ho, J.K.; Jin, R.; Zhang, L.; Shao, H.; Han, C. Silver nanoparticle loaded collagen/chitosan scaffolds promote wound healing via regulating fibroblast migration and macrophage activation. *Sci. Rep.* **2017**, *7*, 10489. [[CrossRef](#)] [[PubMed](#)]
48. Bueno, R.; Marciello, M.; Moreno, M.; Sánchez-Sánchez, C.; Martínez, J.I.; Martínez, L.; Prats-Alfonso, E.; Guimerà-Brunet, A.; Garrido, J.A.; Villa, R.; et al. Versatile graphene-based platform for robust nanobiohybrid interfaces. *ACS Omega* **2019**, *4*, 3287–3297. [[CrossRef](#)]
49. Shrestha, B.; Wang, L.; Zhang, H.; Hung, C.Y.; Tang, L. Gold nanoparticles mediated drug-gene combinational therapy for breast cancer treatment. *Int. J. Nanomed.* **2020**, *15*, 8109–8119. [[CrossRef](#)] [[PubMed](#)]
50. Leu, J.G.; Chen, S.A.; Chen, H.M.; Wu, W.M.; Hung, C.F.; Yao, Y.D.; Tu, C.S.; Liang, Y.J. The effects of gold nanoparticles in wound healing with antioxidant epigallocatechin gallate and alpha-lipoic acid. *Nanomedicine* **2012**, *8*, 767–775. [[CrossRef](#)]
51. Li, Q.; Lu, F.; Zhou, G.; Yu, K.; Lu, B.; Xiao, Y.; Dai, F.; Wu, D.; Lan, G. Silver inlaid with gold nanoparticle/chitosan wound dressing enhances antibacterial activity and porosity, and promotes wound healing. *Biomacromolecules* **2017**, *18*, 3766–3775. [[CrossRef](#)] [[PubMed](#)]
52. Ahmed, T.A.; Aljaeid, B.M. Preparation, characterization, and potential application of chitosan, chitosan derivatives, and chitosan metal nanoparticles in pharmaceutical drug delivery. *Drug Des. Devel. Ther.* **2016**, *10*, 483–507. [[CrossRef](#)] [[PubMed](#)]
53. Riegger, B.R.; Bäurer, B.; Mirzayeva, A.; Tovar, G.E.M.; Bach, M. A systematic approach of chitosan nanoparticle preparation via emulsion crosslinking as potential adsorbent in wastewater treatment. *Carbohydr. Polym.* **2018**, *180*, 46–54. [[CrossRef](#)]
54. Orellano, M.S.; Longo, G.S.; Porporatto, C.; Correa, N.M.; Falcone, R.D. Role of micellar interface in the synthesis of chitosan nanoparticles formulated by reverse micellar method. *Colloids Surf. A Physicochem. Eng. Asp.* **2020**, *599*, 124876. [[CrossRef](#)]
55. Zahraei, M.; Marciello, M.; Lazaro-Carrillo, A.; Villanueva, A.; Herranz, F.; Talelli, M.; Costo, R.; Monshi, A.; Shahbazi-Gahrouei, D.; Amirnasr, M.; et al. Versatile theranostics agents designed by coating ferrite nanoparticles with biocompatible polymers. *Nanotechnology* **2016**, *27*, 255702. [[CrossRef](#)]
56. De la Presa, P.; Luengo, Y.; Multigner, M.; Costo, R.; Morales, M.P.; Rivero, G.; Hernando, A. Study of heating efficiency as a function of concentration, size, and applied field in γ -Fe₂O₃ nanoparticles. *J. Phys. Chem. C* **2012**, *116*, 25602–25610. [[CrossRef](#)]
57. Massart, R. Preparation of aqueous magnetic liquids in alkaline and acidic media. *IEEE Trans. Magn.* **1981**, *17*, 1247–1248. [[CrossRef](#)]
58. Costo, R.; Bello, V.; Robic, C.; Port, M.; Marco, J.F.; Puerto Morales, M.; Veintemillas-Verdaguer, S. Ultrasmall iron oxide nanoparticles for biomedical applications: Improving the colloidal and magnetic properties. *Langmuir* **2012**, *28*, 178–185. [[CrossRef](#)] [[PubMed](#)]
59. Yang, J.; Yin, H.; Jia, J.; Wei, Y. Facile synthesis of high-concentration, stable aqueous dispersions of uniform silver nanoparticles using aniline as a reductant. *Langmuir* **2011**, *27*, 5047–5053. [[CrossRef](#)] [[PubMed](#)]
60. Bastus, N.G.; Comenge, J.; Puntès, V. Kinetically controlled seeded growth synthesis of citrate-stabilized gold nanoparticles of up to 200 nm: Size focusing versus Ostwald ripening. *Langmuir* **2011**, *27*, 11098–11105. [[CrossRef](#)] [[PubMed](#)]
61. Marciello, M.; Rossi, S.; Caramella, C.; Remuñán-López, C. Freeze-dried cylinders carrying chitosan nanoparticles for vaginal peptide delivery. *Carbohydr. Polym.* **2017**, *170*, 43–51. [[CrossRef](#)]
62. Calvo, P.; Remuñán-López, C.; Vila-Jato, J.L.; Alonso, M.J. Chitosan and chitosan/ethylene oxide-propylene oxide block copolymer nanoparticles as novel carriers for proteins and vaccines. *Pharm. Res.* **1997**, *14*, 1431–1436. [[CrossRef](#)]
63. Calvo, P.; Remuñán-López, C.; Vila-Jato, J.L.; Alonso, M.J. Novel hydrophilic chitosan-polyethylene oxide nanoparticles as protein carriers. *J. Appl. Polym. Sci.* **1997**, *63*, 125–132. [[CrossRef](#)]

64. Janes, K.A.; Calvo, P.; Alonso, M.J. Polysaccharide colloidal particles as delivery systems for macromolecules. *Adv. Drug Deliv. Rev.* **2001**, *47*, 83–97. [[CrossRef](#)]
65. Scarabelli, L.; Sanchez-Iglesias, A.; Perez-Juste, J.; Liz-Marzan, L.M. A “Tips and tricks” practical guide to the synthesis of gold nanorods. *J. Phys. Chem. Lett.* **2015**, *6*, 4270–4279. [[CrossRef](#)] [[PubMed](#)]
66. Fan, W.; Yan, W.; Xu, Z.; Ni, H. Formation mechanism of monodisperse, low molecular weight chitosan nanoparticles by ionic gelation technique. *Colloids Surf. B Biointerfaces* **2012**, *90*, 21–27. [[CrossRef](#)]
67. Thandapani, G.; Prasad, S.; Sudha, P.N.; Sukumaran, A. Size optimization and in vitro biocompatibility studies of chitosan nanoparticles. *Int. J. Biol. Macromol.* **2017**, *104*, 1794–1806. [[CrossRef](#)]
68. Rattu, G.; Porcu, E.P.; Fancello, S.; Obinu, A.; Senes, N.; Galleri, G.; Migheli, R.; Gavini, E.; Giunchedi, P. Intranasal delivery of genistein-loaded nanoparticles as a potential preventive system against neurodegenerative disorders. *Pharmaceutics* **2018**, *11*, 8. [[CrossRef](#)]
69. Ahmed, S.B.; Mohamed, H.I.; Al-Subaie, A.M.; Al-Ohali, A.I.; Mahmoud, N.M.R. Investigation of the antimicrobial activity and hematological pattern of nano-chitosan and its nano-copper composite. *Sci. Rep.* **2021**, *11*, 9540. [[CrossRef](#)]
70. Ali, M.E.A.; Aboelfadl, M.M.S.; Selim, A.M.; Khalil, H.F.; Elkady, G.M. Chitosan nanoparticles extracted from shrimp shells, application for removal of Fe(II) and Mn(II) from aqueous phases. *Sep. Sci. Technol.* **2018**, *53*, 2870–2881. [[CrossRef](#)]
71. Jesus, S.; Marques, A.P.; Duarte, A.; Soares, E.; Costa, J.P.; Colaço, M.; Schmutz, M.; Som, C.; Borchard, G.; Wick, P.; et al. Chitosan nanoparticles: Shedding light on immunotoxicity and hemocompatibility. *Front. Bioeng. Biotechnol.* **2020**, *8*, 100. [[CrossRef](#)]
72. Omid, S.; Kakanejadifard, A. Modification of chitosan and chitosan nanoparticle by long chain pyridinium compounds: Synthesis, characterization, antibacterial, and antioxidant activities. *Carbohydr. Polym.* **2019**, *208*, 477–485. [[CrossRef](#)]
73. Shawkat, S.M.; Al-Jawasim, M.; Khaleefah, L.S. Extending shelf life of pasteurized milk via chitosan nanoparticles. *J. Pure Appl. Microbiol.* **2019**, *13*, 2471. [[CrossRef](#)]
74. Ing, L.Y.; Zin, N.M.; Sarwar, A.; Katas, H. Antifungal activity of chitosan nanoparticles and correlation with their physical properties. *Int. J. Biomater.* **2012**, *2012*, 632698. [[CrossRef](#)]
75. Lustriane, C.; Dwivany, F.M.; Suendo, V.; Reza, M. Effect of chitosan and chitosan-nanoparticles on post harvest quality of banana fruits. *J. Plant Biotechnol.* **2018**, *45*, 36–44. [[CrossRef](#)]
76. Des Jardins-Park, H.E.; Foster, D.S.; Longaker, M.T. Fibroblasts and wound healing: An update. *Regen. Med.* **2018**, *13*, 491–495. [[CrossRef](#)] [[PubMed](#)]
77. Sengul, A.B.; Asmatulu, E. Toxicity of metal and metal oxide nanoparticles: A review. *Environ. Chem. Lett.* **2020**, *18*, 1659–1683. [[CrossRef](#)]
78. Petkovsek, Z.; Elersic, K.; Gubina, M.; Zgur-Bertok, D.; Starcic Erjavec, M. Virulence potential of *Escherichia coli* isolates from skin and soft tissue infections. *J. Clin. Microbiol.* **2009**, *47*, 1811–1817. [[CrossRef](#)] [[PubMed](#)]
79. Ali Khan, Z.; Jamil, S.; Akhtar, A.; Mustehsan Bashir, M.; Yar, M. Chitosan based hybrid materials used for wound healing applications—A short review. *Int. J. Polym. Mater. Polym. Biomater.* **2020**, *69*, 419–436. [[CrossRef](#)]